ACS ES&T Air

Open Access

pubs.acs.org/estair

Article

Intercomparison of Methane Emission Rate Methods Using Aerial and Ground-Level Mobile Monitoring at New York State Landfills

Alexandra M. Catena, Lee T. Murray, Jie Zhang, Eric M. Leibensperger, Roisin Commane, Mackenzie L. Smith, Margaret J. Schwab, Andrew Hallward-Driemeier, Matthew L. Loman, and James J. Schwab*

Cite This: https://doi.org/10.1021/acsestair.5c00145

Read Online

ACCESS | Metrics & More | Article Recommendations | Supporting Information

ABSTRACT: Methane concentrations were measured at major New York State (NYS) landfills in 2021 and 2022 using both aerial and ground-level monitoring from a mobile research lab (MRL) to determine facility emission rates. These emission rates were estimated by a mass balance method using Gauss's Theorem and a Gaussian Plume Dispersion (GPD) method. Three separate emission rates were calculated for each of the facilities when data was available, two of which were calculated using both the GPD and mass balance methods from the MRL data, and the third using the more rigorous aircraft data and mass balance method, which was used as the reference estimate. Both MRL GPD and mass balance methods come with considerable uncertainty, which is mainly driven by stability class and distance for the GPD and plume height for the mass balance. All but one of the GPD estimates fell within the uncertainty range of the aircraft estimates and estimated a CH_4 emission rate range of 262−3896 kg h^{-1}. The MRL mass balance estimates, however, proved to be quite different from the aircraft aside from one case with an estimated range of 463−6285 kg h^{-1}. The poor agreement between the MRL mass balance and the aircraft reduces confidence in these estimates. The observations were also compared to the 2021 and 2022 self-reported EPA Greenhouse Gas Reporting Program (GHGRP) Inventory. The aircraft estimates were, on average, 2.2× greater than the GHGRP while the MRL estimates were more variable in comparison with the inventory. This study provides information on these different estimation methods and will help improve and inform the GHG emissions inventory.

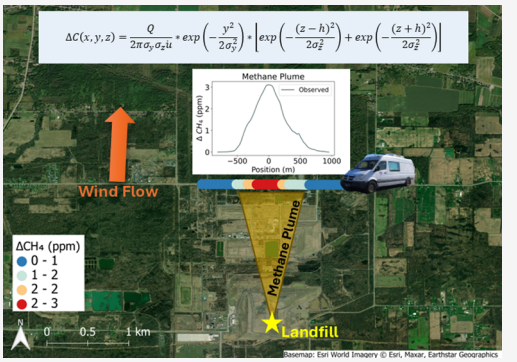

KEYWORDS: *methane, landfills, emission estimates, Gaussian Plume Dispersion, mass balance, greenhouse gas inventory*

1. INTRODUCTION

Methane (CH_4) is a potent global greenhouse gas (GHG) and is the leading gaseous contributor to global warming behind carbon dioxide (CO_2).[1] Compared on a molecule-to-molecule basis, methane is more impactful than CO_2 by a factor of about ∼84× over a 20-year time scale, which underscores the importance of this GHG. The methane oxidation chain also leads to secondary formation of background ozone (O_3), an important pollutant and GHG itself, followed by eventual oxidation into CO_2.[2,3] Anthropogenic sources account for about 60% of global methane emissions, which are dominated by the agriculture, energy, and waste sectors.[4,5] These sectors have shown to emit methane at an accelerating rate over the past decade with expected continued growth throughout the next decade.[6]

Landfills have come under increased scrutiny due to their large methane emissions. The US waste sector accounted for 2.7% of total GHG emissions by CO_2 equivalent (CO2e) using the 100-year global warming potential (GWP) metric as reported in the draft 2023 Environmental Protection Agency (EPA) Greenhouse Gas Inventory (GHGI),[7] with methane emissions as the largest contributor to GHGs from this sector. All landfills that emit over 25,000 MT of CO2e are required to report to the EPA Greenhouse Gas Reporting Program (GHGRP) under 40 CFR Part 98 subpart HH for municipal solid waste (MSW) landfills.[8] MSW landfills subject to the GHGRP are also required to have a composite liner, landfill gas capture system, leachate collection system, and daily and intermediate covering of the landfilled material.[8]

Reducing fugitive methane emissions from landfills is one of the top priorities of New York State's (NYS) 2019 Climate Leadership and Community Protection Act to reduce statewide GHG emissions.[9] The NYS Department of Environmental Conservation (DEC) reported that landfills accounted

Received: April 23, 2025
Revised: November 21, 2025
Accepted: November 21, 2025

for 37% of total statewide methane emissions in 2022 based on the bottom-up emissions inventory.[10] Landfill methane emissions in NYS are calculated and reported using methods provided by the 2006 IPCC Guidelines and its supplements and refinements (2019 IPCC Refinements).[10−12] These calculations use a bottom-up First Order Decay (FOD) model, which depend on site-specific factors including waste mass, decay parametrizations, emission factors, and gas capture management.[10,13] While the EPA GHGRP and the NYS GHG Inventory follow similar methodologies in estimating landfill methane emissions, the GHGRP provides facility-level emissions while the latter provides statewide totals.

Estimating methane emissions at landfills can be quite complex due to the high spatial and temporal heterogeneity in emissions coupled with landfill topography.[13−16] Temporal variations can be due to a variety of factors including diurnal fluctuations in pressure, ambient temperature, wind, or soil temperature[17−19] and seasonal variation in methane oxidation.[20,21] Spatial variability at landfills could be due to landfill topography[22] or cover soil properties, like its thickness, porosity, or oxidation potential.[14,23] Methane can also leak through cracks in the soil due to drought or erosion.[13,24] Other factors that lead to variation in methane, especially between landfill facilities, are different management or operational practices, which include LFG recovery systems and extraction, leachate storage or treatment, or use of liners or covers.[14,25] At the same time, emissions are confined to a limited geographical area, typically much smaller than a wetland, agricultural facility, or urban area.

The significant variation in emissions between landfills makes it challenging to use a one-size-fits-all method to estimate a sitewide methane emission rate. Although the inventory landfill emission estimation methodology does involve some facility-specific inputs like waste mass or measured methane recovery, default values and assumptions are still used in many cases, which can lead to major uncertainties and inaccuracies. Several past studies have demonstrated through direct measurements that the methodology used for the emissions inventory does not account for all methane emissions from landfills.[13,26−28]

There is a need for direct measurements and top-down emission estimates for individual landfill sites to improve accuracy of emissions inventories and ensure representation of variability in emissions through temporal, operational, and technological changes. To determine accuracy of emissions inventories, bottom-up approaches are increasingly being reconciled with top-down approaches, which use direct measurements to infer emission rates through inverse modeling.[29] However, some top-down approaches, such as the tracer release or flux chamber methods, do not infer emission rates through inverse modeling.

Given the complexity of estimating landfill emissions, there are several different methods of inverse modeling, which mostly depend on the type of measurement platform used, including satellites,[24,30−32] aircraft,[13,28,33] tower measurements,[26] unmanned aerial vehicles,[34−36] or ground-level monitoring.[15,33,36,37] Each have their own advantages and disadvantages and are suitable for different measurement campaigns that depend on factors such as distance from the landfill, spatial vastness of measurements, duration and location of measurements, and travel speed of measurement platform.[38]

This study aims to determine the applicability and efficacy of two separate methods using ground-level mobile monitoring, including a Gaussian Plume Dispersion (GPD) method[2] and a mass balance method, which applies Gauss's Theorem.[39,40] These estimates will be referenced against a third emission rate estimated from a Gauss's Theorem mass balance method using aircraft observations.[41] The GPD method estimates the emission rate of a facility using the downwind CH_4 mixing ratio enhancement, distance from the source, atmospheric stability, and wind speed as the plume is dispersed normally in the horizontal and vertical directions. The simplest formulation of this method occurs when the winds are perpendicular to the downwind transect.[42,43] The method does not require the emission plume height, making it well suited for ground-based monitoring measurements.

The aircraft mass balance method estimates the emission rate by calculating the flux divergence through an enclosed boundary around the facility from the surface up to the plume height.[33,40] It is estimated by numerically integrating the horizontal wind vector with the methane mixing ratio enhancement at every point of measurement around the facility and summing up over each height level up to the top of the plume. The sum of each of these levels is the total net flux of the facility. Since the plume height is not available for the mobile monitoring data, the method slightly diverges between the aircraft and mobile monitoring estimates. This involves a novel use of ground-based mobile lab measurements to apply the Gauss's Theorem mass balance method.

In total, this paper investigates three separate emission rate estimations for five landfills in NYS − one GPD estimate using ground-level mobile monitoring data, and two mass balance estimates using aircraft and ground-level mobile monitoring data. The goals of this paper are to understand the differences between these emission estimation methods, determine whether ground-level mobile monitoring can deliver comparable estimates to the more costly and complete aircraft measurements, and compare the observations from this study to the EPA GHGRP Inventory. The results from this study will help inform the methane emissions inventory, pinpoint areas of need for climate mitigation and policy, and provide guidance and information to scientists and researchers on different methane estimation methods.

2. METHODS

The study was conducted to determine spatial variability, identify hot spots, and when possible, determine emission rates of methane throughout NYS using mobile measurements. It consisted of three separate field campaigns carried out in June 2021, November 2021, and July 2022. Each deployment involved ∼ 14 days of measurements. The measurements were primarily carried out by the Atmospheric Science Research Center mobile research laboratory (MRL), with intermittent simultaneous aircraft measurements completed by the scientific research aviation company, Scientific Aviation, now known as Champion X, during some of the June and November 2021 deployments. The Scientific Aviation sampling and emission estimation results are described in Catena et al.[41] Sampling for calculating the GPD method involves numerous repeated downwind transects to measure the maximum concentration (or plume), while the Gauss's Theorem mass balance method requires full loops around the facility, resulting in fewer transects of the plume.

https://doi.org/10.1021/acsestair.5c00145
ACS EST Air XXXX, XXX, XXX−XXX

As stated above, emission rates were calculated using two separate methods, including a GPD method and a mass balance approach using Gauss's Theorem. Emission estimates using the aircraft measurements were calculated by Scientific Aviation from a mass balance approach using Gauss's Theorem,[40,41] which is expected to be the most accurate due to its ability to sample from the lowest allowed flight level (150 m above ground level) up to the plume height, thus the MRL GPD and mass balance estimates will be referenced against the aircraft mass balance estimates. Table 1 lists the landfill facilities and dates visited for this paper and whether there were simultaneous measurements during sampling. It also lists the nearest NYS Mesonet site. Landfill site descriptions on cover types, approximate acreages, and other characteristics can be found in Section S1 of the supplement. A map of the measurements are also provided for each site in the supplement. Figure 1 is a map of all the landfills analyzed in this paper.

Table 1. Sample Date at each of the Visited Landfill Sites and Associated NYS Mesonet Site Used[a]

facility	dates visited	simultaneous aircraft and MRL measurements?	NYS mesonet site
Modern Landfill, Inc. (43.21205, −78.97421)	6/15/2021	yes	Burt
	11/21/2021	yes	Buffalo
	7/23/2022	no	
High Acres Landfill (43.08332, −77.37310)	7/24/2022	no	Rush
			Clifton Springs
	7/27/2022	no	South Bristol
Seneca Meadows Landfill (42.92436, −76.84487)	6/16/2021	yes	Waterloo
	11/17/2021	yes	
	7/25/2022	no	
	7/28/2022	no	
Riga Mill Seat Landfill (43.05674, −77.93424)	6/14/2021	no	Batavia
	6/15/2021	yes	Brockport
	7/26/2022	no	Rush
			York
Ontario County Landfill (42.85460, −77.08148)	6/16/2021	yes	Waterloo
	7/25/2022	no	Clifton Springs

[a]Each site also indicates whether there were simultaneous measurements of aircraft and mobile research lab (MRL) sampling.

2.1. Measurement Platforms. *2.1.1. Mobile Research Lab.* The main mode of measurement was through the ASRC MRL, using a 2007 Dodge Sprinter van. This van has been used several times in the past for similar monitoring deployments.[44−46] The MRL was equipped with GHG analyzers, described below, and trace gas analyzers, including O_3 and NO_2. The power system consisted of eight Lithium ion batteries with a total capacity of 13 kWh to power the analyzers, a GPS, and a weather sensor mounted on the roof of the vehicle. Maximum vehicle speeds reached up to 20 m s^{-1} with an average downwind speed of 7 m s^{-1}. Data was measured at 1 s.

Methane was measured using a high time-resolution Aerodyne Dual Quantum-Cascade LAS (QCLS), which uses tunable infrared laser direct absorption spectroscopy through astigmatic multipass absorption cells. The Dual QCLS uses two multiplexed lasers to measure CH_4, C_2H_6, CO, N_2O, CO_2, and H_2O. Commane et al.[47] determined the CH_4 precision to be 0.227 ppbv at 1 Hz and 0.072 ppbv for 10 s averaged[47] data. The analyzer is further described elsewhere.[47,48] The van was also equipped with a Picarro G2204, which is a cavity ring-down spectrometer that uses a near-infrared laser to measure the absorption spectra of air samples. The Picarro G2204 measured CH_4 and hydrogen sulfide (H_2S). The fact sheet lists the 1σ, 5 s precision of 1 ppb and 1σ, 5 min precision of 0.5 ppb for CH_4 (https://www.picarro.com/environmental/g2204_analyzer_datasheet). The Picarro G2204 had a consistently lower baseline compared to the QCLS, which was more frequently calibrated. The Picarro G2204 was thus corrected to the National Oceanographic and Atmospheric Administration (NOAA)/World Meteorological Organization (WMO) CH_4 scale (described below) through evaluation of data, which resulted in a baseline correction of 0.1 ppm but no change in span.

Meteorology parameters were measured using an Airmar 220WX, including temperature, relative humidity, pressure, and wind direction and speed. However, post analysis concluded major inaccuracies in the wind speed and direction parameters,[49] and the unreliability precluded its use. Instead, wind data was retrieved from the nearest NYS Mesonet Station,[50] which are referenced in Table 1.

Sampled air was drawn in through the inlet just above the driver's side between the roof and the windshield. Analyzer clocks were corrected for both drift over the deployment and gas transit time from the inlet to match the van GPS. Analyzer spans were calibrated with a two-tank calibration pre- and post-deployment and the zero-offset of the QCLS was measured consistently throughout the campaign. Calibration tanks are traceable to standards calibrated by the Central Calibration Laboratory (CCL) at the NOAA Global Monitoring Laboratory in Boulder, CO, which maintains the WMO CH_4 scale (WMO X2004A). All data analysis and mapping software was done through Python and QGIS, respectively.

2.1.2. Aircraft. Aircraft measurements were carried out during the June and November 2021 deployments.[41] The aircraft was flown by Scientific Aviation (now Champion X), which is a Colorado-based scientific research company, and it was equipped with several trace gas analyzers that measured CH_4, CO_2, CO, and H_2O using a Picarro 2401 with calibrations done inflight, along with wind speed and direction, temperature, pressure, relative humidity, and GPS. Further descriptions and discussion of the Scientific Aviation aircraft, analyzer precision and accuracy, and met data can be found elsewhere.[40,51−55]

2.2. Methane Emission Rate Methods. As mentioned above, two different methods were used to calculate the CH_4 emission rate from the facilities visited during the study. These methods included a Gaussian Plume Dispersion (GPD) method and mass balance approach using Gauss's Theorem. Both are described in the following sections.

2.2.1. MRL Gaussian Plume Dispersion. The Gaussian Plume Dispersion model estimates a downwind mixing ratio as a function of distance, emission rate, wind speed, and vertical and horizontal dispersion rates from a point source.[2] A Gaussian distribution of the plume is assumed as it disperses in the horizontal and vertical directions. The GPD calculation involves the emission rate of the facility Q, mean wind speed $\bar{u}$ at the height of the facility per transect, enhancement above background ΔC at receptor location, x distance from source to receptor, y and z positions of the plume, facility height h, and

https://doi.org/10.1021/acsestair.5c00145
ACS EST Air XXXX, XXX, XXX−XXX

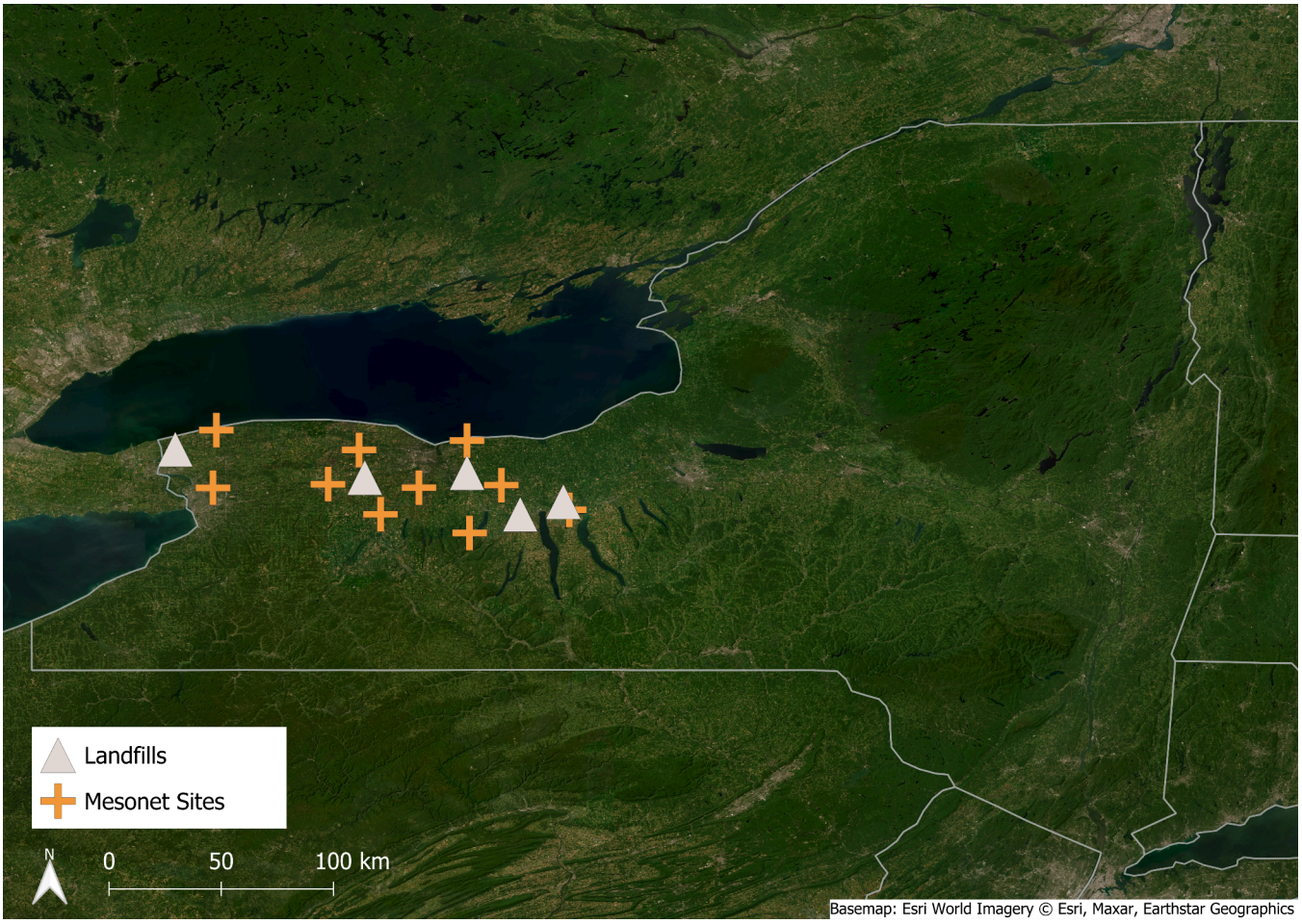

Figure 1. Map of all landfills analyzed in this study in western New York.

stability parameters σ_y and σ_z in the following equation, which accounts for reflection at the surface[2]:

$$\Delta C(x, y, z) = \frac{Q}{2\pi\sigma_y\sigma_z\bar{u}}\exp\left(-\frac{y^2}{2\sigma_y^2}\right)\left[\exp\left(-\frac{(z-h)^2}{2\sigma_z^2}\right) + \exp\left(-\frac{(z+h)^2}{2\sigma_z^2}\right)\right] \quad (1)$$

The GPD method was calculated using two separate methods including the peak enhancement emission rate (PGPD), which only uses the peak enhancement of the Gaussian-fitted plume, and the integrated emission rate (IGPD), which considers the entire measured plume. While both upwind and downwind measurements were recorded from circling the facility on adjacent roads, the GPD calculations only involved the enhanced methane above background on the downwind transect. The downwind transect was defined as the road most perpendicular to the plume where the maximum mixing ratios of methane were detected.

Peak Enhancement Gaussian Plume Dispersion. The observed data were fitted to a Gaussian distribution and the peak of that distribution was used in eq 2 below to calculate the peak enhancement GPD emission rate. As done in previous GPD studies,[56−58] using only the peak concentration enhancement above background, ΔC_{peak}, of each Gaussian-fitted plume per transect allowed for a simplified version of the model. In this case the analysis is always normalized around the centerline of the plume, which is the location of the peak concentration (position 0). The y-dispersion term, $\exp\left(-\frac{y^2}{2\sigma_y^2}\right)$, then becomes 1 since $y = 0$. Treating the facility as a point source and solving for the total emission rate of the facility, Q, then becomes

$$Q = \frac{2\pi\sigma_y\sigma_z\bar{u}\Delta C_{peak}(x, 0, 0)}{\left[\exp\left(-\frac{(z-h)^2}{2\sigma_z^2}\right) + \exp\left(-\frac{(z+h)^2}{2\sigma_z^2}\right)\right]} \quad (2)$$

Integrated Gaussian Plume Dispersion. The integrated GPD is calculated by integrating the entire observed plume (ΔC_{obs}) along the transect. Unlike the PGPD, the observed mixing ratio enhancements above background were used in the analysis, as opposed to the Gaussian-fitted values. The plumes were centered at $y = 0$ for each transect. Letting

$$G = \frac{\exp\left(-\frac{y^2}{2\sigma_y^2}\right)\left[\exp\left(-\frac{(z-h)^2}{2\sigma_z^2}\right) + \exp\left(-\frac{(z+h)^2}{2\sigma_z^2}\right)\right]}{2\pi\sigma_y\sigma_z\bar{u}} \quad (3)$$

eq 1 can be simplified to

$$\Delta C_{obs} = QG \quad (4)$$

Rearranging eq 4 and summing along the transect results in

https://doi.org/10.1021/acsestair.5c00145
ACS EST Air XXXX, XXX, XXX−XXX

$$Q = \frac{\sum \Delta C_i \mathrm{d}l_i}{\sum G_i \mathrm{d}l_i} \quad (5)$$

where ΔC_i is the concentration at point i in [kg m^{-3}], $\mathrm{d}l_i$ is the change in length per time step at point i in [m], and G_i is the model response per unit emission rate in $\left[\frac{\mathrm{kgm}^{-3}}{\mathrm{kgs}^{-1}}\right]$ or [s m^{-3}], and as defined above in eq 3, at point i. eq 5 was determined for each transect and the average of all transects was the total emission rate for each facility. Given that the integrated approach accounts for multiple enhancements within the plume and utilizes actual observations, the integrated method values were used in further analysis. A more in-depth comparison of the two approaches is included in Section S4 of the Supplement.

The enhancement above background was computed by using the fifth percentile as the background threshold per transect, upwind of the source. The inlet height was taken as the height of the inlet on the roof of the van, which is 3.3 m. The height of the facility is taken as the landfill elevation, which is determined from Google Earth.

The wind speed at 10 m is converted to the wind speed at the height of the landfill, which is done through the equation[59]:

$$\mathrm{wind}_{\mathrm{landfillheight}} = \mathrm{wind}_{10\mathrm{m}}\left(\frac{\mathrm{height}_{\mathrm{landfill}}}{10}\right)^{\alpha} \quad (6)$$

where α is determined from a lookup table that depends on if the facility is in a rural or urban area. The winds were retrieved from the closest New York State (NYS) Mesonet station,[50] which were measured from a 10 m tower.

The dispersion terms, σ_y and σ_z, were determined from the Pasquill-Gifford stability class,[42,43] with stability class, A, being the most unstable up to stability class, F, as the most stable and depend on distance from the source, x. The stability class was determined based on the solar insolation and surface wind speed average during the measurement period, which were both reported from the NYS Mesonet. Given the determined stability class and the distance between the plume and the source, the dispersion parameters, σ_y and σ_z, were calculated using the following equations:

$$\sigma_y = ax^b$$
$$\sigma_z = cx^d + f \quad (7)$$

Where x was the distance from the source to the peak enhancement above background, and the a, b, c, d, and f terms were determined from a lookup table depending on the stability class.[60]

The GPD modeled emission rate was calculated using eq 5 and a 10,000 iteration Monte Carlo simulation allowing for variation of 9% for distances less than 1 km or 100 m for distances greater than 1 km, 4% for wind speed, 8% for σ_y, and 11% for σ_z for each downwind transect. These variations were based on average variations for each of the observations. An average of ± 20 m was used for crosswind variation (change in y coordinate), which was based on the standard deviation of the plume center location between the transects. The empirical uncertainty is also an output of the Monte Carlo simulation calculation. The total GPD emission rate for each landfill was the averaged value for all transects.

2.2.2. GPD Assumptions and Uncertainty. The peak concentration and integrated Gaussian Plume Dispersion method used here has several assumptions and uncertainties. Due to high spatial variability and unknown location of emission sources within landfills,[13,16] a potential source of error is introduced if these facilities are assumed to be point sources. The dependence on distance is illustrated in the dispersion parameter calculations (eq 7), which defines the plume dispersion. Variation in source locations can result in a large range of dispersion parameters due to different distance lengths, and the method is more well suited to measurement distances that are far enough away for the plume to disperse down to the surface and become well mixed.[16] Scarpelli et al.,[24] determined that the working face of a landfill was the most probable location of emissions. Also, a study done by Fredenslund et al.,[57] calculated two separate emission rates from landfills using a simple Gaussian Plume Dispersion model as described here (and treating it as a point source) and a tracer gas dispersion method. They found that the Gaussian modeled rates were 72% that of the tracer emission rates with an R^2 = 0.765.[57] Following both Scarpelli et al.[24] and Fredenslund et al.,[57] and for the sake of simplicity, the landfills are treated as point sources in this analysis, and the center of the working face was chosen as the location of the point source for the GPD calculations. Because of this, each downwind transect would ideally show a single Gaussian plume, while actual observations sometimes show multiple peaks. Since the integrated approach would account for multiple peaks within a plume, this method was used instead of the peak enhancement.

In addition to the uncertainty in the source location and distance, the assigned stability class also plays into the uncertainty in the GPD model. As seen in eq 7, the dispersion parameters, σ_y and σ_z, also depend on stability class as the a, b, c, d, and f coefficients are based on stability class determination. Choosing between stability classes can result in significantly different numbers. Riddick et al.[61] found the greatest uncertainty in the GPD model was due to variation in the stability parameters leading to an uncertainty of 41%.[61]

Another assumption of this model is a favorable wind speed and direction that is constant and perpendicular to the downwind transect. This leads to uncertainty in the emission rate due to the varying nature of wind. Multiple peaks in the observed methane profile could therefore result from the changing wind direction, rather than additional sources in the landfill. Confidence level is highest when winds are orthogonal to transects and the landfill point source is directly upwind of transect.

This method assumes a normal distribution of the plume in the vertical and horizontal directions for a single point source along the perpendicular transect to the plume. Some instances of downwind transects do not capture the entirety of the plume, which was mostly due to the vehicle having to turn down a different, nonperpendicular road. These measurements were not analyzed using the GPD method. Mobile measurements taken at a slow but steady ground speed are also necessary to acquire a clear, normally distributed plume, so any stationary data was omitted from the calculation. It should also be noted that a normal distribution will leave out multiple observed plumes within a single transect, which hinders the ability to account for multiple sources within the landfill. Choosing to only account for the peak plume concentration (and treating this at a point source) may underestimate the emission rate, thus the integrated GPD calculation was used for comparisons to the mass balance methods, as discussed in S4 of the Supplement.

https://doi.org/10.1021/acsestair.5c00145
ACS EST Air XXXX, XXX, XXX−XXX

2.2.3. Mass balance Using Gauss's Theorem for Aircraft and MRL. The mass balance approach was applied to both the MRL and aircraft measurements. There are slight modifications to the MRL mass balance equation, which are described below.

Aircraft Mass Balance. The dispersion of emissions from the facility into the well-mixed boundary layer are sampled by the aircraft as it circles the facility in a virtual cylinder from the lowest allowed flight level up to above the plume.[40] Gauss's Theorem is then applied to the observed data including horizontal wind speed and direction and measured methane mixing ratios to calculate the flux divergence through the virtual cylinder. The contribution from the facility is then determined by integrating the outward horizontal flux around this virtual cylinder, which can be seen in eq 8:

$$Q_c = \left\langle \frac{\partial m}{\partial t} \right\rangle + \int_0^{z_{\max}} \oint c' u_h \cdot \hat{n} \, dl \, dz \tag{8}$$

where Q_c is the emission rate, $z_{\max}$ is the top of the sampling height, c' is the deviation from the mean concentration for each loop, such that $C = \overline{c} + c'$, where C is the measured concentration and $\overline{c}$ is the mean concentration per loop, u_h is the horizontal wind vector, $\hat{n}$ is the outward pointing unit vector, dl is the change in length per sample, and dz is the change in height between each loop around the facility. The volume mixing ratio is converted to a mass mixing ratio using the ideal gas law, and then multiped by the altitude-dependent density to obtain mass concentration. The storage term, $\left\langle \frac{\partial m}{\partial t} \right\rangle$ is calculated as the time rate of change of the average mass concentration within the sampled volume throughout the entire period of measurements.

The aircraft only sampled during the June and November 2021 deployments at a select number of facilities.[41] Scientific Aviation also calculated emission estimates for the sites visited, which are listed below. The standard deviations of the horizontal flux through each aggregated height bin were calculated as the uncertainty for each of the height levels. These were then summed in quadrature to get the total uncertainty for each estimate.

MRL Mass Balance. Applying MRL measurements to a loop integral mass balance method using Gauss's Theorem is a novel approach to estimate emissions in contrast to the GPD method described above. To account for variation in height levels up to the top of the plume, the mean density is calculated at 100 different levels from the surface to the top of the plume height. The modified MRL mass balance equation is as follows in eq 9:

$$Q_c = \left\langle \frac{\partial m}{\partial t} \right\rangle + \sum_0^L \Delta c (1e^{-6}) \rho \frac{MW_{CH4}}{MW_{AIR}} (u_n n_i + v_n n_j) dl Z_P \tag{9}$$

where $\left\langle \frac{\partial m}{\partial t} \right\rangle$ is the time rate of change of the average mass concentration within the sampled volume throughout the entire period of measurements, Δc is the methane mixing ratio enhancement above background per loop in parts per million (ppm), which is multiplied by the scaling factor $1e^{-6}$ to convert to a mole fraction from ppm, ρ kg m^{-3} is the mean density, which was calculated in an iteration over 100 different layers from the surface up to the plume height based on surface temperature, surface pressure, and scale height, which was then averaged to get the mean density from the equation $\rho = \rho_{\text{surface}} e^{-\text{layer}/H}$, where H is the scale height and layer is one of the 100 layers or heights of measurement per iteration. $\frac{MW_{CH4}}{MW_{AIR}}$ g mol^{-1} g mol^{-1} is the ratio of molecular weight of CH_4 to the molecular weight of dry air, $u_n n_i + v_n n_j$ is the mean u and v wind components multiplied by the i and j components of the vehicle heading in units of m s^{-1}, dl is the distance traveled for every time step m over the loop, L, and Z_P is the plume height. The first term of eq 9, the storage term, $\left\langle \frac{\partial m}{\partial t} \right\rangle$, is estimated as the time rate of change of the average mass concentration of the entire sampled volume surrounding the sampled facility. Consistent with previous studies,[62,63] we have not included the storage term, due to it being small and highly uncertain. The storage term is discussed in detail in Section S3 of the Supplement.

2.2.4. Mass Balance Uncertainty. While the aircraft mass balance method can be categorized as the most rigorous method to determine emission rates due to its ability to sample the whole plume without needing access to the landfill itself, there are several limitations to the method as well. Due to flight restrictions, the aircraft cannot fly below 150 m AGL, hence the entire section of atmosphere from the landfill surface up to 150 m does not have directly measured data. To make up for this, all parameters of eq 8 were assumed constant from the lowest flight level down to the surface, which leads to uncertainty. There is also the difficultly of singling out a point source among several other adjacent sources, which is especially a problem in urban areas.

One very challenging issue with the MRL mass balance calculation was determining the plume height. Since this was not available via direct measurements for the MRL measurements, the plume height was estimated from relationships observed in the aircraft measurements. The aircraft plume heights were determined as the height above ground level (AGL) at which the methane enhancement was no longer detected. For those deployments where there are simultaneous measurements from the aircraft and the MRL, the empirically determined measured aircraft plume height was scaled to apply to the MRL measurements as a scaled plume height by accounting for differing horizontal distances between the source and sample locations for the MRL and the aircraft. This was done by taking the ratio of the horizontal distances from the aircraft and from the MRL to the point source. This ratio was then multiplied by the estimated plume height from the aircraft.

To estimate the plume height for the days without the aircraft-measured plume height, a linear relationship was first derived using the available 2021 aircraft data from Catena et al.[41] That aircraft data involved a total of 36 sample days, 25 of which were analyzed for that study, with various stability classes. Combining those 36 aircraft plume height measurements from that data set with the stability classifications from the GPD method, a linear regression was fitted between the aircraft-measured plume height (x-axis) and the product of the calculated σ_z from eq 7 and the distance to the source solely using the aircraft measurements (y-axis). This linear regression was then applied to the MRL data for days without simultaneous aircraft measurements to estimate a fitted plume height using the distance and calculated σ_z dispersion parameter from eq 7 using the MRL measurements (fitted plume height).

https://doi.org/10.1021/acsestair.5c00145
ACS EST Air XXXX, XXX, XXX−XXX

Table 2 compares the scaled plume heights from the aircraft and the fitted plume heights used for the MRL calculations.

Table 2. Plume Height Comparisons between the Scaled Plume Height from the Aircraft and the Fitted Plume Height Used for the Mobile Research Lab (MRL) Mass Balance Calculations[a]

sample site and date	scaled plume height AGL (m)	fitted plume height AGL (m)	MRL distance to source (m)	stability class	σ_z
Riga Mill Seat 06/14/21		469	1594	B	183
Modern 06/15/21	201		620	B	66
Riga Mill Seat 06/15/21	285		1512	C	89
Ontario 06/16/21	109		390	B	38
Seneca 06/16/21	268		1040	B	115
Seneca 11/17/21	249		2090	C	119
Modern 11/21/21	362		2386	C	135
Modern 07/23/22		292	2290	C	130
High Acres 07/24/22		283	760	B	80
Ontario 07/25/22		243	336	B	34
Seneca 07/25/22		399	1350	B	152
Riga Mill Seat 07/26/22		458	1561	B	178
High Acres 07/27/22		330	767	A	273
Seneca 07/28/22		186	2240	D	53

[a]The MRL distance to the source, stability classification, and calculated dispersion parameter σ_z are also displayed. The fitted heights were used when no scaled plume height was available.

The calculation involved the scaled plume height from the aircraft when it was available, whereas the fitted heights are used for the 2022 data and Riga Mill Seat on 06/14/2021.

Downsides to using this method include the issue that the linear regression analysis does not include observations below 150 m due to flight restrictions. This leaves out details on the plume profile and thus reduces accuracy for days when there were no flight measurements. This regression is also based on a relatively few number of observations, which may not be representative of true conditions.

The uncertainty was calculated as the standard deviation between each loop. For the sample days with three or fewer loops, an averaged uncertainty was applied from days with four or more loops, which averaged to 40%.

3. RESULTS AND DISCUSSION

The emission rate estimates at each of the selected landfills for both aircraft and MRL measurements are shown in Table 3 and will be discussed in Section 3.1. Given that the aircraft methodology has been established in the literature, both MRL estimates will be referenced against the aircraft estimates to determine efficacy. Figure 2 compares the methods against each other. Table 3 also lists the 2021 and 2022 EPA GHGRP inventory estimates for each of the landfills. The GPD results in this table use the integrated plume method, as described above. The comparisons between the observations and the inventory will be discussed in Section 3.2.

3.1. Emission Rate Method Comparison. *3.1.1. GPD Comparisons to the Aircraft Estimates.* Table 3 and Figure 2 depict the intercomparison between the GPD and mass balance methods for both measurement platforms. The GPD estimates are similar to the aircraft estimates in that almost all GPD estimates were within the uncertainty range of the aircraft estimates, when available, aside from one estimate at Seneca Meadows Landfill (Seneca) on 6/16/21. These similar GPD emission rate estimate calculations involved favorable sampling and meteorological conditions in that they were able to capture the whole plume from background to background and had completed multiple transects, all while winds were mostly perpendicular to the downwind transects.

The source of the largest uncertainty was due to adjusting the stability class to one class more unstable (A − most unstable, F − most stable), which was also the case in the Riddick et al.[61] study. There were several instances when it was difficult to choose between stability classes, with considerably different results. For example, the weather conditions during sampling at Modern Landfill, Inc. (Modern) on 07/23/22 determined the stability class to be right on the cusp between B or C. Using stability class, B, resulted in an emission rate of 1665 kg h^{-1} while stability class, C, resulted in an emission rate

Table 3. Methane Emission Rates Estimated from Using a Mass Balance and Gaussian Plume Dispersion (GPD) from Aircraft[41] and Mobile Research Lab (MRL) Measurement Platforms for all Sampled Landfills[a]

landfill	date	mass balance−aircraft (kg/h)	Gaussian Plume Dispersion−MRL (kg/h)	mass balance−MRL (kg/h)	2021 EPA GHGRP (kg/h)	2022 EPA GHGRP (kg/h)
Riga Mill Seat	6/14/2021			1748 ± 769	673	
Modern	6/15/2021	785 ± 246		3047 ± 1341	1343	
Riga Mill Seat	6/15/2021	902 ± 295		1385 ± 610	673	
Ontario	6/16/2021	983 ± 306	818 ± 74	1566 ± 689	434	
Seneca	6/16/2021	2789 ± 815	3725 ± 190	3806 ± 1674	726	
Seneca	11/17/2021	3099 ± 708	2651 ± 89	3312 ± 934	726	
Modern	11/21/2021	1277 ± 342	1288 ± 91	2451 ± 1316	1343	
Modern	7/23/2022		735 ± 33	1156 ± 380		1663
High Acres	7/24/2022		3896 ± 235	6285 ± 3396		776
Ontario	7/25/2022		712 ± 81	1638 ± 132		511
Seneca	7/25/2022		1843 ± 94	2945 ± 1345		736
Riga Mill Seat	7/26/2022		262 ± 11	463 ± 204		576
High Acres	7/27/2022		1681 ± 111	1738 ± 697		776
Seneca	7/28/2022		1486 ± 68	3610 ± 1221		736

[a]The 2021 and 2022 self-reported Environmental Protection Agency Greenhouse Gas Reporting Program (EPA GHGRP) inventory estimates are also included.

https://doi.org/10.1021/acsestair.5c00145
ACS EST Air XXXX, XXX, XXX−XXX

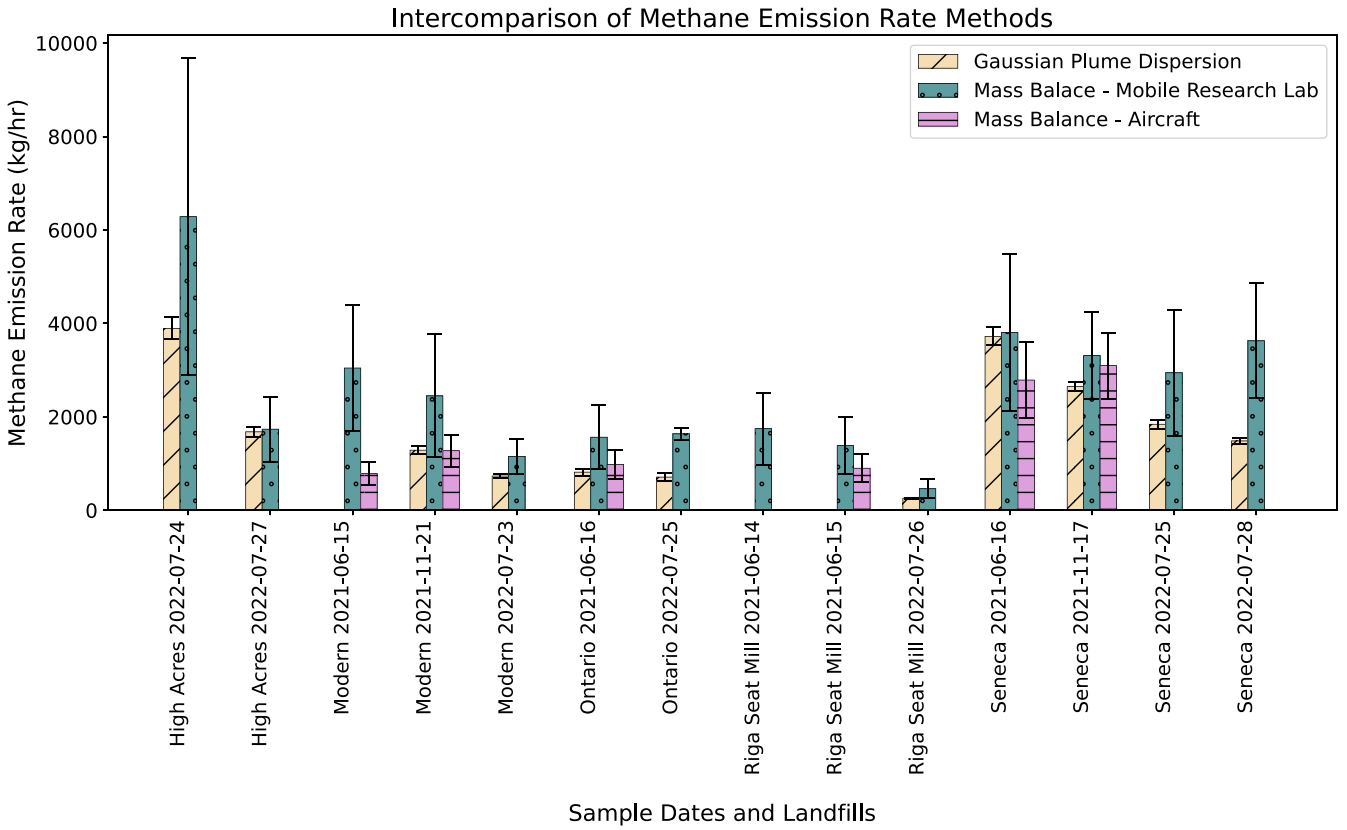

Figure 2. Comparisons between each of the three estimated emission rates including the Gaussian Plume Dispersion and mass balance methods using Gauss's Theorem using the mobile research lab measurements and the mass balance method using the aircraft measurements.

of 735 kg h^{-1}. While the meteorology measurements from the Buffalo and Burt Mesonet sites could result in either class, conditions from that day were mostly cloudy, which lowered the solar insolation at that site, making C the more likely determined stability class.

Distance is also an important consideration for the GPD method. When the dimensions of the working face of the landfill (source area) were comparable to the distance between the roadway and the source, the plume is unable to become well-mixed before sampling. As mentioned above, the sampling needs to take place far enough away for a landfill to be considered a point source thus the relatively short distances for the Ontario County Landfill (Ontario) measurements may not be the most accurate. An important uncertainty in this method is treating the landfill as a point source and deciding which location to use as the point of emission. Seneca Landfill had two separate working face locations (Figure S15) during the time of measurements. Using the two separate locations as the point of emission resulted in an average 38% difference. This significant difference highlights the major influence of distance on this method and brings up a valid concern when attempting to determine the best location of a point source when using the point source approximation. Modern Landfill, however, also had two working face locations with an estimated emission rate percent difference of only about 5% using the two separate locations. However, the working face locations at Seneca are ~1100 m apart while the working face locations at Modern are only 300 m apart, which could explain the small percent difference at Modern.

Additionally, and as mentioned above, treating the landfill as a point source and only including the peak concentration of the entire transect can possibly lead to an underestimation of the emission rate due to leaving out other possible sources within the landfill. This underscores the importance of measuring far enough away from the source where the plume can become mixed enough to be treated like a point source. Given this limitation of using the peak enhancement, the integrated approach was used instead, which is further explained in the Supplement.

While there are a number of assumptions and sometimes difficulty assigning stability class, the GPD method is suitable due to the few inputs it requires. It does not consider plume height, only involves one side of the facility (can save time rather than driving around the entire facility), and is relatively straightforward.

Like other GPD studies,[21,57,64] we encountered meteorological and logistical conditions and situations that were problematic enough that several attempted measurements were excluded. Some instances of this were due to a combination of wind direction and road geometry causing the plume to traverse over road corners as opposed to across a straight transect and thus distorting the Gaussian shape of the plume. An example of this occurred at Riga Mill Seat on 6/14/21 and 6/15/21 and Modern on 6/15/21 when the plume was captured on a curved part of the road leading to an incomplete capture of the plume throughout the entire day of measurements. Over the three deployment periods, an additional 11 sample dates were attempted but excluded mainly due to too short of a distance to the landfill. The necessity to use existing roads meant that the measurement distance was often too close. For a few cases, sampling was also done within the perimeter of the landfill itself.

https://doi.org/10.1021/acsestair.5c00145
ACS EST Air XXXX, XXX, XXX−XXX

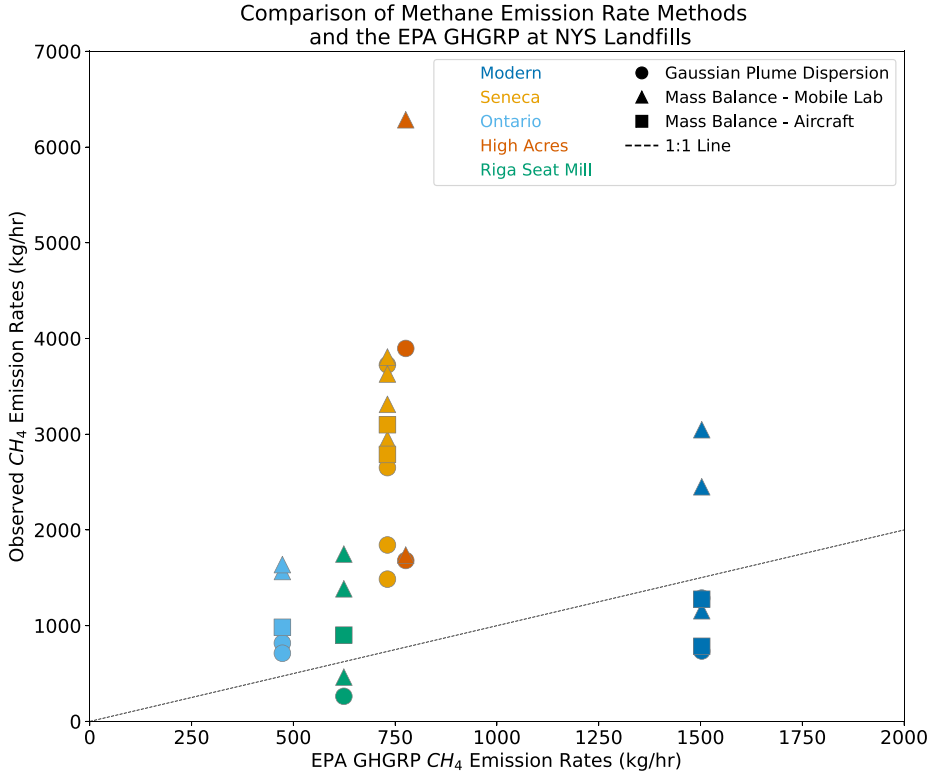

Figure 3. Comparisons between each of the methods at every landfill with the self-reported Environmental Protection Agency (EPA) Greenhouse Gas Reporting Program (GHGRP) methane (CH_4) inventory estimate. The Gaussian Plume Dispersion (GPD) estimates are shown with the circle markers, the mass balance mobile research lab estimates are shown with the triangle markers, and the mass balance aircraft estimates are shown with the square markers. The average EPA GHGRP value is used between 2021 and 2022. Uncertainties for MRL and aircraft estimates are in Table 3.

3.1.2. MRL Mass Balance Comparisons to the Aircraft. Estimating the emission rates using the mass balance method for the MRL measurements proved to be more challenging, which was mostly due to the inability to determine an accurate estimate of the plume height. This ultimately proved to be the main source of uncertainty in these estimates. For the measurements in 2021 where the MRL and aircraft measurements were available, only Seneca on 11/17/21 had an MRL mass balance emission rate within the uncertainty range of the aircraft estimates. Since an accurate plume height could not be determined for the ground measurements, the plume height was fitted using the aircraft measurements, as mentioned above in Section 2.2.4 and thus, these estimates are less reliable and more uncertain. Given the poor agreement between the mass balance MRL and the aircraft estimates, the mass balance method may not be ideal for estimating emission rates using ground-level mobile monitoring data, unless conditions are favorable and an accurate determination of the plume height is known. However, even for the 2021 measurements with a scaled plume height from the aircraft, the MRL mass balance estimated fluxes were still dissimilar to the aircraft method. Upper air measurements are vital for ensuring the highest accuracy in the MRL mass balance method.

The MRL mass balance estimates were higher than all MRL GPD estimates. The most similar estimates were Seneca on 06/16/2021 and High Acres on 07/27/2022. However, some of the MRL mass balance estimates were significantly different than the GPD estimates, particularly for both days at Ontario, Seneca on 07/28/2022, Riga Mill Seat on 07/26/2022, and Modern on 11/21/2021. The large range in values for both MRL estimates follow similar studies done by Kumar et al.,[21] Lan et al.,[65] and Olaguer et al.,[36] all of which used a GPD method to estimate landfill emissions. Kumar et al.[21] measured one landfill 11 times over 3 years and found a range in emissions from 17 to 292 kg h^{-1}. Lan et al.[65] sampled at four different landfills with an estimated range of 86−2087 kg h^{-1}. Lastly, Olaguer et al.[36] estimated an average emission rate of 500 kg h^{-1} at two landfills using a combination of mobile laboratory and drone measurements.[36]

3.1.3. Other Uncertainties. In addition to uncertainties in the calculations, there were also some challenges involved with on-road measurements. Vehicles can only take public roads, which may not be conducive for capturing the whole plume, especially if the landfill is too far away (or too close) or there are obstacles such as buildings or trees. There can also be a problem if meteorological conditions are unfavorable. For example, if only one side of a landfill can be measured, it must be downwind of the landfill during sampling. Attempting to encircle a landfill on the adjacent roads can also lead to suboptimal loop shapes, which may not be so much of an issue for the mass balance method (as long as it is closed) but more of a problem for the GPD method, which was the case for the Modern 6/15/21 estimate. The GPD works best when the downwind transect is completely straight and perpendicular to the wind flow as this can fully capture the Gaussian shape of the plume. Since these are also ground-based measurements, upper-level parameters needed for these analyses are either estimated or assumed constant, such as concentration, wind speed and direction, and density. While some variations to these variables may compensate with increasing height, the

https://doi.org/10.1021/acsestair.5c00145
ACS EST Air XXXX, XXX, XXX−XXX

mass balance method is based on a vertical integral; thus, having all parameters measured as a function of height allows a more accurate estimate.

Therefore, there is considerable uncertainty in the MRL estimates. However, the GPD method shows promising results, indicating that ground-level mobile monitoring can estimate landfill emissions, given favorable conditions and sampling locations. Mobile research laboratories have the advantage that they are more cost-effective and require less time and planning compared to aircraft measurements.

3.2. Comparisons between Observations and EPA GHGRP Inventory. Figure 3 and Table 3 also show comparisons with the 2021 and 2022 EPA GHGRP landfill estimates. As found in Catena et al.,[41] the observed landfill aircraft estimates are, on average, 2.2 times higher than the reported inventory estimate. The aircraft estimates were higher for every landfill except at Modern Landfill, which had the highest self-reported inventory estimate for both 2021 and 2022. More details on the aircraft comparisons to the self-reported inventory are described in Catena et al.[41]

The MRL GPD and mass balance estimates showed more variability in how they compared to the self-reported inventory estimates. All MRL estimates were higher than the inventory at Seneca, High Acres, and Ontario for both methods. Both MRL estimates were lower than the self-reported inventory at Modern on 07/23/2022 and Riga Mill Seat on 07/26/2022. The 11/21/2021 GPD estimate at Modern was the most comparable estimate overall to the inventory. The MRL mass balance estimates seem to be biased high and were greater than the inventory for the most part. One exception to this is Riga Mill Seat on 07/26/2022, which was the only instance where the self-reported inventory number was within the uncertainty range of the MRL mass balance estimate. There exist uncertainties in both the GPD and mass balance estimates, which are due in large part to the stability class determination for the GPD and the plume height for the mass balance method. Addressing these uncertainties will improve these estimates.

There was also a variation in emissions between the landfills themselves. The 2021 MRL Seneca and Riga Mill Seat estimates were higher than the 2022 estimates for both methods. High Acres also showed a significant difference between the two sample days for both methods. A probable reason for these differences between and within landfills could be attributed to landfill operations and different cover types or meteorology, as these factors are the main drivers behind landfill emissions.[13,29,66−70] Landfills have a mixture of covers, including daily, intermediate, and final covers that have various thicknesses and multilayered systems. Each of these covers have different methane oxidation rates and can have significantly different influences on emission rates.[67] Previous studies have indicated that methane oxidation increases and methane emissions decrease with increased cover, i.e. daily to intermediate to final.[67,71,72] Spokas et al.[73] determined that landfill covers with thin or fewer layers (daily and intermediate) result in higher emissions and lower oxidation rates than covers with multilayered systems, as required for final covers. A study done by California Polytechnical Institute studied a number of California landfills and found that methane emissions increased with the least amount of cover.[72] They found that daily covers using alternative materials, particularly covers using autofluff, had the highest methane fluxes as that material is usually thin and porous. The final covers had the least amount of emission due to the high soil content and use of geosynthetics. Modern, Seneca, and Riga Mill Seat all used some percentage of autofluff as alternative daily cover, according to their 2022 annual reports.[74−76] As mentioned above, Scarpelli et al.[24] also found that satellite measurements indicated a high emission rate from the working face, or daily cover, from landfills.[24] There is also variation within the different intermediate cover types, whether the cover involves soil, a geomembrane, vegetation, or any combination. A previous study found that a thicker 45 cm thick vegetated intermediate cover resulted in fewer emissions than the thinner 15 cm thick nonvegetated intermediate cover.[77] A description of each of the landfills from this study is presented in Section S1 of the Supplement.

4. CONCLUSIONS

To improve the NYS emissions inventory, emission rates were calculated at several landfills in 2021 and 2022 using both ground-level mobile monitoring and aircraft measurements. To the best of our knowledge, this is the first time emission rate estimates have been calculated using direct measurements from these NYS landfill facilities. This paper focused on the intercomparison of using two separate methods to estimate emission rates using both measurement platforms. Three emission rates were calculated for each of the facilities − a GPD method and mass balance approach using Gauss's Theorem for the MRL data and a mass balance method using Gauss's Theorem using the aircraft data. While each method has its own level of uncertainty, the aircraft estimates are likely the most accurate due to their ability to sample most of the plume at several different altitudes, whereas the MRL measurements are limited to ground level. Therefore, the MRL estimates were referenced against the aircraft estimates for accuracy determination. Besides one case, the GPD estimates were within the uncertainty ranges of the aircraft estimates, making this a viable option for estimating emission rates. There is considerable uncertainty, however, especially in regard to stability class determination and location of and distance to the source. The MRL mass balance estimates, on the other hand, were not as similar, with only one emission rate within the uncertainty range of the aircraft estimates. The variation and uncertainty in the MRL mass balance estimates mostly came from not having an accurate measurement of the plume height. The plume height estimated in this work does not seem to be an accurate representation of the true plume height. The poor agreement in the MRL estimates gives low confidence to this method as compared to the GPD method. There were also considerable emission differences between and within the landfills, which can most likely be attributed to operational differences and fluctuations in meteorological parameters.

The observations were also compared to the self-reported EPA GHGRP inventory. The aircraft estimates were higher than the self-reported inventory for every site except Modern Landfill, which had the highest 2021 and 2022 GHGRP inventory estimate. Seneca Landfill was the only site where all three observations were higher than the self-reported inventory estimate. Both estimates which used observed MRL measurements were higher than the self-reported inventory estimate for all samples at Seneca, High Acres, and Ontario. This shows that the methods and protocol used to comply with state regulations and guidelines are underestimating actual emissions from landfills in the GHG Inventory. The results from

https://doi.org/10.1021/acsestair.5c00145
ACS EST Air XXXX, XXX, XXX−XXX

this study provide guidance and information on these two different estimation methods. These emission estimates will also help inform the NYS GHG Inventory and thus improve climate policy and regulation in reducing methane emissions.

■ ASSOCIATED CONTENT

Data Availability Statement

The data described in this manuscript can be found at the temporary link: http://datadryad.org/share/vKagQrLEBGAdsZMDyxAcniIyCNlkWvV9Oq6iuClrjIk

Supporting Information

The Supporting Information is available free of charge at https://pubs.acs.org/doi/10.1021/acsestair.5c00145.

Information on each of the landfills from this study; map of sampling routes and measurements; parameters used for the equations; storage term; and integrated and peak Gaussian Plume Dispersion method differences (PDF)

■ AUTHOR INFORMATION

Corresponding Author

James J. Schwab − *Atmospheric Sciences Research Center, University at Albany, State University of New York, Albany, New York 12203, United States;* orcid.org/0000-0003-1343-4695; Email: jschwab@albany.edu

Authors

Alexandra M. Catena − *Atmospheric Sciences Research Center, University at Albany, State University of New York, Albany, New York 12203, United States;* orcid.org/0000-0003-4369-7736

Lee T. Murray − *Department of Earth and Environmental Sciences, University of Rochester, Rochester, New York 14620, United States;* orcid.org/0000-0002-3447-3952

Jie Zhang − *Atmospheric Sciences Research Center, University at Albany, State University of New York, Albany, New York 12203, United States;* orcid.org/0000-0003-2935-9220

Eric M. Leibensperger − *Department of Physics and Astronomy, Ithaca College, Ithaca, New York 14850, United States*

Roisin Commane − *Lamont-Doherty Earth Observatory, Columbia University, Palisades, New York 10964, United States; Department of Earth and Environmental Sciences, Columbia University, New York, New York 10027, United States;* orcid.org/0000-0003-1373-1550

Mackenzie L. Smith − *Scientific Aviation, Now Champion X, The Woodlands, Texas 77381, United States*

Margaret J. Schwab − *Atmospheric Sciences Research Center, University at Albany, State University of New York, Albany, New York 12203, United States*

Andrew Hallward-Driemeier − *Lamont-Doherty Earth Observatory, Columbia University, Palisades, New York 10964, United States; Department of Earth and Environmental Sciences, Columbia University, New York, New York 10027, United States;* orcid.org/0000-0003-1125-288X

Matthew L. Loman − *Department of Earth and Environmental Sciences, University of Rochester, Rochester, New York 14620, United States;* orcid.org/0000-0002-9749-3600

Complete contact information is available at: https://pubs.acs.org/10.1021/acsestair.5c00145

Author Contributions

This study was conceptualized by J.J.S., L.M., R.C., and E.L. The MRL setup and preparation for fieldwork were done by M.J.S., J.Z., J.J.S., and A.M.C. MRL data collection and fieldwork were carried out by J.Z., A.M.C., R.C., M.L., and A.H. All aircraft fieldwork and aircraft emission calculations were completed by M.S. MRL data analysis and emission calculations were done by A.M.C., L.M., E.L., R.C., and J.J.S. Manuscript developed by A.M.C. with extensive contributions from all coauthors.

Funding

This work has been supported through the New York State Energy Research and Development Authority (NYSERDA) Contract 156227.

Notes

The authors declare no competing financial interest.

■ ACKNOWLEDGMENTS

We acknowledge the support by the New York State Energy Research and Development Authority (NYSERDA, contract: 156227). Any opinion expressed in this article does not necessarily reflect those of NYSERDA or the State of New York. We also acknowledge the support and assistance from Dirk Felton and Oliver Rattigan from New York State Department of Environmental Conservation for lending the Picarro G2204 for this project. Lastly, thank you to Dr. Joseph Marto for aiding in the MRL fieldwork.

■ REFERENCES

(1) Myhre, G.; Shindell, D.; Bréon, F.; Collins, W.; Fuglestvedt, J.; Huang, J.; Koch, D.; Lamarque, J.; Lee, D.; Mendoza, B.; Nakajima, T.; Robock, A.; Stephens, G.; Takemura, T.; Zhang, H.; Qin, D.; Plattner, G.; Tignor, M.; Allen, S.; Boschung, J.; Nauels, A.; Xia, Y.; Bex, V.; Midgley, P. Anthropogenic and Natural Radiative Forc-Ing. In: *Climate Change 2013: The Physical Science Basis. Contribution of Working Group I*; Cambridge University Press: Cambridge, UK, 2013.

(2) Seinfeld, J. H.; Pandis, S. N. *Atmospheric Chemistry and Physics - From Air Pollution to Climate Change*, 3rd ed.; John Wiley & Sons, Ltd.: Hoboken, NJ, 2016.

(3) Shindell, D.; Sadavarte, P.; Aben, I.; Bredariol, T. de O.; Dreyfus, G.; Höglund-Isaksson, L.; Poulter, B.; Saunois, M.; Schmidt, G. A.; Szopa, S.; Rentz, K.; Parsons, L.; Qu, Z.; Faluvegi, G.; Maasakkers, J. D. The Methane Imperative. *Front. Sci.* **2024**, *2*, No. 1349770.

(4) IPCC. In *Climate Change 2023: Synthesis Report. Contribution of Working Groups I, II and III to the Sixth Assessment Report of the Intergovernmental Panel on Climate Change*, Arias, P.; Bustamante, M.; Elgizouli, I.; Flato, G.; Howden, M.; Méndez-Vallejo, C.; Pereira, J. J.; Pichs-Madruga, R.; Rose, S. K.; Saheb, Y.; Sánchez Rodríguez, R.; Ürge-Vorsatz, D.; Xiao, C.; Yassaa, N.; Romero, J.; Kim, J.; Haites, E. F.; Jung, Y.; Stavins, R.; Birt, A.; Ha, M.; Orendain, D. J. A.; Ignon, L.; Park, S.; Park, Y.; Reisinger, A.; Cammaramo, D.; Fischlin, A.; Fuglestvedt, J. S.; Hansen, G.; Ludden, C.; Masson-Delmotte, V.; Matthews, J. B. R.; Mintenbeck, K.; Pirani, A.; Poloczanska, E.; Leprince-Ringuet, N.; Péan, C., Eds.; Geneva, Switzerland, 2023.

(5) IEA. *Methane Tracker 2021*; Paris, 2021. https://www.iea.org/reports/methane-tracker-2021.

(6) United Nations Environment Programme and Climate and Clean Air Coalition. *Global Methane Assessment: Benefits and Costs of Mitigating Methane Emissions*; United Nations Environment Programme: Nairobi, 2021.

(7) US EPA. *DRAFT US-GHG-Inventory-2025-Chapter-7-Waste*. https://www.regulations.gov/document/EPA-HQ-OAR-2024-0591-0002 (accessed September 2, 2025).

(8) CFR. eCFR:: 40 CFR Part 98 Subpart HH -- Municipal Solid Waste Landfills. https://www.ecfr.gov/current/title-40/chapter-I/

subchapter-C/part-98/subpart-HH#p-98.343(a)(1) (accessed July 16, 2022).
(9) New York State Climate Action Council. *New York State Climate Action Council Scoping Plan*, 2022. climate.ny.gov/ScopingPlan%0D.
(10) NYS DEC. *2024 NYS GREENHOUSE GAS EMISSIONS REPORT*, 2024. https://dec.ny.gov/sites/default/files/2024-12/summaryreportnysghgemissionsreport.pdf.
(11) IPCC. In *Refinement to the 2006 IPCC Guidelines for National Greenhouse Gas Inventories*, Calvo Buendia, E.; Tanabe, K.; Kranjc, A.; Baasansuren, J.; Fukuda, M.; Ngarize, S.; Osako, A.; Pyrozhenko, Y.; Shermanau, P.; Federici, S., Eds.; IPCC: Switzerland, 2019.
(12) IPCC. In *IPCC Guidelines for National Greenhouse Gas Inventories*; Eggelston, S.; Buendia, L.; Miwa, K.; Ngara, T.; Tanabe, K., Eds.; Institute for Global Environmental Strategies (IGES) for the IPCC: Japan, 2006.
(13) Cusworth, D. H.; Duren, R. M.; Ayasse, A. K.; Jiorle, R.; Howell, K.; Aubrey, A.; Green, R. O.; Eastwood, M. L.; Chapman, J. W.; Thorpe, A. K.; Heckler, J.; Asner, G. P.; Smith, M. L.; Thoma, E.; Krause, M. J.; Heins, D.; Thorneloe, S. Quantifying Methane Emissions from United States Landfills. *Science (1979)* **2024**, *383* (6690), 1499−1504.
(14) Delgado, M.; López, A.; Esteban, A. L.; Lobo, A. Some Findings on the Spatial and Temporal Distribution of Methane Emissions in Landfills. *J. Clean Prod* **2022**, *362*, No. 132334.
(15) Rees-White, T. C.; Mønster, J.; Beaven, R. P.; Scheutz, C. Measuring Methane Emissions from a UK Landfill Using the Tracer Dispersion Method and the Influence of Operational and Environmental Factors. *Waste Manage.* **2019**, *87*, 870−882.
(16) Mønster, J.; Kjeldsen, P.; Scheutz, C. Methodologies for Measuring Fugitive Methane Emissions from Landfills − A Review. *Waste Manage.* **2019**, *87*, 835−859.
(17) Delkash, M.; Zhou, B.; Han, B.; Chow, F. K.; Rella, C. W.; Imhoff, P. T. Short-Term Landfill Methane Emissions Dependency on Wind. *Waste Management* **2016**, *55*, 288−298.
(18) Poulsen, T. G.; Christophersen, M.; Moldrup, P.; Kjeldsen, P. Relating Landfill Gas Emissions to Atmospheric Pressure Using Numerical Modelling and State-Space Analysis. *Waste Management & Research: The Journal for a Sustainable Circular Economy* **2003**, *21* (4), 356−366.
(19) Uyanik, İ.; Özkaya, B.; Demir, S.; Çakmakci, M. Meteorological Parameters as an Important Factor on the Energy Recovery of Landfill Gas in Landfills. *Journal of Renewable and Sustainable Energy* **2012**, *4* (6), No. 063135.
(20) Christophersen, M.; Kjeldsen, P.; Holst, H.; Chanton, J. Lateral Gas Transport in Soil Adjacent to an Old Landfill: Factors Governing Emissions and Methane Oxidation. *Waste Management & Research: The Journal for a Sustainable Circular Economy* **2001**, *19* (6), 595−612.
(21) Kumar, P.; Caldow, C.; Broquet, G.; Shah, A.; Laurent, O.; Yver-Kwok, C.; Ars, S.; Defratyka, S.; Gichuki, S. W.; Lienhardt, L.; Lozano, M.; Paris, J.-D.; Vogel, F.; Bouchet, C.; Allegrini, E.; Kelly, R.; Juery, C.; Ciais, P. Detection and Long-Term Quantification of Methane Emissions from an Active Landfill. *Atmos Meas Tech* **2024**, *17* (4), 1229−1250.
(22) Rachor, I. M.; Gebert, J.; Gröngröft, A.; Pfeiffer, E.-M. Variability of Methane Emissions from an Old Landfill over Different Time-scales. *Eur. J. Soil Sci.* **2013**, *64* (1), 16−26.
(23) Abushammala, M. F. M.; Basri, N. E. A.; Elfithri, R.; Younes, M. K.; Irwan, D. Modeling of Methane Oxidation in Landfill Cover Soil Using an Artificial Neural Network. *J. Air Waste Manage Assoc* **2014**, *64* (2), 150−159.
(24) Scarpelli, T. R.; Cusworth, D. H.; Duren, R. M.; Kim, J.; Heckler, J.; Asner, G. P.; Thoma, E.; Krause, M. J.; Heins, D.; Thorneloe, S. Investigating Major Sources of Methane Emissions at US Landfills. *Environ. Sci. Technol.* **2024**, *58* (49), 21545−21556.
(25) Ayandele, E.; Cusworth, D.; Duren, R.; Fisher, B.; Huffman, K.; Jungclaus, M.; Tseng, E. *Key Strategies for Mitigating Methane Emissions from Municipal Solid Waste*, **2022**. https://rmi.org/insight/mitigating-methane-emissions-from-municipal-solid-waste/.
(26) Lamb, B. K.; Cambaliza, M. O. L.; Davis, K. J.; Edburg, S. L.; Ferrara, T. W.; Floerchinger, C.; Heimburger, A. M. F.; Herndon, S.; Lauvaux, T.; Lavoie, T.; Lyon, D. R.; Miles, N.; Prasad, K. R.; Richardson, S.; Roscioli, J. R.; Salmon, O. E.; Shepson, P. B.; Stirm, B. H.; Whetstone, J. Direct and Indirect Measurements and Modeling of Methane Emissions in Indianapolis. *Indiana. Environ. Sci. Technol.* **2016**, *50* (16), 8910−8917.
(27) Lu, X.; Jacob, D. J.; Wang, H.; Maasakkers, J. D.; Zhang, Y.; Scarpelli, T. R.; Shen, L.; Qu, Z.; Sulprizio, M. P.; Nesser, H.; Bloom, A. A.; Ma, S.; Worden, J. R.; Fan, S.; Parker, R. J.; Boesch, H.; Gautam, R.; Gordon, D.; Moran, M. D.; Reuland, F.; Villasana, C. A. O.; Andrews, A. Methane Emissions in the United States, Canada, and Mexico: Evaluation of National Methane Emission Inventories and 2010−2017 Sectoral Trends by Inverse Analysis of in Situ (GLOBALVIEWplus CH4 ObsPack) and Satellite (GOSAT) Atmospheric Observations. *Atmos Chem. Phys.* **2022**, *22* (1), 395−418.
(28) Ren, X.; Salmon, O. E.; Hansford, J. R.; Ahn, D.; Hall, D.; Benish, S. E.; Stratton, P. R.; He, H.; Sahu, S.; Grimes, C.; Heimburger, A. M. F.; Martin, C. R.; Cohen, M. D.; Stunder, B.; Salawitch, R. J.; Ehrman, S. H.; Shepson, P. B.; Dickerson, R. R. Methane Emissions From the Baltimore-Washington Area Based on Airborne Observations: Comparison to Emissions Inventories. *Journal of Geophysical Research: Atmospheres* **2018**, *123* (16), 8869−8882.
(29) National Academies of Sciences, T. *Improving Characterization of Anthropogenic Methane Emissions in the United States*, **2018**.
(30) Balasus, N.; Jacob, D. J.; Maxemin, G.; Jenks, C.; Nesser, H.; Maasakkers, J. D.; Cusworth, D. H.; Scarpelli, T. R.; Varon, D. J.; Wang, X. Satellite Monitoring of Annual US Landfill Methane Emissions and Trends. *Environmental Research Letters* **2025**, *20* (2), No. 024007.
(31) Nesser, H.; Jacob, D. J.; Maasakkers, J. D.; Lorente, A.; Chen, Z.; Lu, X.; Shen, L.; Qu, Z.; Sulprizio, M. P.; Winter, M.; Ma, S.; Bloom, A. A.; Worden, J. R.; Stavins, R. N.; Randles, C. A. High-Resolution US Methane Emissions Inferred from an Inversion of 2019 TROPOMI Satellite Data: Contributions from Individual States, Urban Areas, and Landfills. *Atmos Chem. Phys.* **2024**, *24* (8), 5069−5091.
(32) Duren, R. M.; Thorpe, A. K.; Foster, K. T.; Rafiq, T.; Hopkins, F. M.; Yadav, V.; Bue, B. D.; Thompson, D. R.; Conley, S.; Colombi, N. K.; Frankenberg, C.; McCubbin, I. B.; Eastwood, M. L.; Falk, M.; Herner, J. D.; Croes, B. E.; Green, R. O.; Miller, C. E. California's Methane Super-Emitters. *Nature* **2019**, *575* (7781), 180−184.
(33) Yeşiller, N.; Hanson, J. L.; Manheim, D. C.; Newman, S.; Guha, A. Assessment of Methane Emissions from a California Landfill Using Concurrent Experimental, Inventory, and Modeling Approaches. *Waste Management* **2022**, *154*, 146−159.
(34) Allen, G.; Hollingsworth, P.; Kabbabe, K.; Pitt, J. R.; Mead, M. I.; Illingworth, S.; Roberts, G.; Bourn, M.; Shallcross, D. E.; Percival, C. J. The Development and Trial of an Unmanned Aerial System for the Measurement of Methane Flux from Landfill and Greenhouse Gas Emission Hotspots. *Waste Management* **2019**, *87*, 883−892.
(35) Daugėla, I.; Suziedelyte Visockiene, J.; Kumpiene, J. Detection And Analysis Of Methane Emissions From A Landfill Using Unmanned Aerial Drone Systems And Semiconductor Sensors. *Detritus* **2020**, *10*, 127−138.
(36) Olaguer, E.; Jeltema, S.; Gauthier, T.; Jermalowicz, D.; Ostaszewski, A.; Batterman, S.; Xia, T.; Raneses, J.; Kovalchick, M.; Miller, S.; Acevedo, J.; Lamb, J.; Benya, J.; Wendling, A.; Zhu, J. Landfill Emissions of Methane Inferred from Unmanned Aerial Vehicle and Mobile Ground Measurements. *Atmosphere (Basel)* **2022**, *13* (6), No. 983.
(37) Bogner, J.; Spokas, K.; Burton, E.; Sweeney, R.; Corona, V. Landfills as Atmospheric Methane Sources and Sinks. *Chemosphere* **1995**, *31* (9), 4119−4130.
(38) Environment Agency. *Quantifying methane emissions using inverse dispersion modelling*. https://assets.publishing.service.gov.uk/media/65649e2b62180b0012ce821f/Quantifying_methane_

https://doi.org/10.1021/acsestair.5c00145
ACS EST Air XXXX, XXX, XXX−XXX

emissions_using_inverse_dispersion_modelling_-_report.pdf (accessed September 2, 2025).
(39) Koene, E. F. M.; Brunner, D.; Kuhlmann, G. On the Theory of the Divergence Method for Quantifying Source Emissions From Satellite Observations. *J. Geophys. Res.: Atmos.* **2024**, *129* (12), No. e2023JD039904.
(40) Conley, S.; Faloona, I.; Mehrotra, S.; Suard, M.; Lenschow, D. H.; Sweeney, C.; Herndon, S.; Schwietzke, S.; Pétron, G.; Pifer, J.; Kort, E. A.; Schnell, R. Application of Gauss's Theorem to Quantify Localized Surface Emissions from Airborne Measurements of Wind and Trace Gases. *Atmos. Meas. Tech* **2017**, *10*, 3345−3358.
(41) Catena, A. M.; Smith, M. L.; Murray, L. T.; Leibensperger, E. M.; Zhang, J.; Schwab, M. J.; Schwab, J. J. Aerial Estimates of Methane and Carbon Dioxide Emission Rates Using a Mass Balance Approach in New York State. *Earth Syst. Sci. Data* **2025**, *17* (9), 4555−4568.
(42) Gifford, F. A. Use of Routine Meteorological Observations for Estimating Atmospheric Dispersion. *Nucl. Saf.* **1961**, *2*, 44−57.
(43) Turner, B. *Workbook of Atmospheric Dispersion Estimates*. https://nepis.epa.gov/Exe/ZyPURL.cgi?Dockey=9100JEIO.txt (accessed September 2, 2025).
(44) Zhang, J.; Lance, S.; Marto, J.; Sun, Y.; Ninneman, M.; Crandall, B. A.; Wang, J.; Zhang, Q.; Schwab, J. J. Evolution of Aerosol Under Moist and Fog Conditions in a Rural Forest Environment: Insights From High-Resolution Aerosol Mass Spectrometry. *Geophys. Res. Lett.* **2020**, *47* (19), No. e2020GL089714.
(45) Zhang, J.; Lance, S.; Marto, J.; Sun, Y.; Ninneman, M.; Crandall, B. A.; Wang, J.; Zhang, Q.; Schwab, J. J. Evolution of Aerosol Under Moist and Fog Conditions in a Rural Forest Environment: Insights From High-Resolution Aerosol Mass Spectrometry. *Geophys. Res. Lett.* **2020**, *47* (19), No. e2020GL089714.
(46) Zhang, J.; Ninneman, M.; Joseph, E.; Schwab, M. J.; Shrestha, B.; Schwab, J. J. Mobile Laboratory Measurements of High Surface Ozone Levels and Spatial Heterogeneity During LISTOS 2018: Evidence for Sea Breeze Influence. *Journal of Geophysical Research: Atmospheres* **2020**, *125* (11), 31961.
(47) Commane, R.; Hallward-Driemeier, A.; Murray, L. T. Intercomparison of Commercial Analyzers for Atmospheric Ethane and Methane Observations. *Atmos Meas Tech* **2023**, *16* (5), 1431−1441.
(48) Li, J.; Parchatka, U.; Fischer, H. Development of Field-Deployable QCL Sensor for Simultaneous Detection of Ambient N2O and CO. *Sens Actuators B Chem.* **2013**, *182*, 659−667.
(49) Leibensperger, E. M.; Konieczny, M.; Weil, M. D. Uncertainty in the Mobile Observation of Wind. *Atmosphere (Basel)* **2023**, *14* (5), No. 765.
(50) Brotzge, J. A.; Wang, J.; Thorncroft, C. D.; Joseph, E.; Bain, N.; Bassill, N.; Farruggio, N.; Freedman, J. M.; Hemker, K.; Johnston, D.; Kane, E.; McKim, S.; Miller, S. D.; Minder, J. R.; Naple, P.; Perez, S.; Schwab, J. J.; Schwab, M. J.; Sicker, J. A Technical Overview of the New York State Mesonet Standard Network. *J. Atmos Ocean Technol.* **2020**, *37* (10), 1827−1845.
(51) Conley, S. A.; Faloona, I. C.; Lenschow, D. H.; Karion, A.; Sweeney, C. A Low-Cost System for Measuring Horizontal Winds from Single-Engine Aircraft. *J. Atmos Ocean Technol.* **2014**, *31* (6), 1312−1320.
(52) Peischl, J.; Karion, A.; Sweeney, C.; Kort, E. A.; Smith, M. L.; Brandt, A. R.; Yeskoo, T.; Aikin, K. C.; Conley, S. A.; Gvakharia, A.; Trainer, M.; Wolter, S.; Ryerson, T. B. Quantifying Atmospheric Methane Emissions from Oil and Natural Gas Production in the Bakken Shale Region of North Dakota. *Journal of Geophysical Research: Atmospheres* **2016**, *121* (10), 6101−6111.
(53) Smith, M. L.; Kort, E. A.; Karion, A.; Sweeney, C.; Herndon, S. C.; Yacovitch, T. I. Airborne Ethane Observations in the Barnett Shale: Quantification of Ethane Flux and Attribution of Methane Emissions. *Environ. Sci. Technol.* **2015**, *49* (13), 8158−8166.
(54) Karion, A.; Sweeney, C.; Kort, E. A.; Shepson, P. B.; Brewer, A.; Cambaliza, M.; Conley, S. A.; Davis, K.; Deng, A.; Hardesty, M.; Herndon, S. C.; Lauvaux, T.; Lavoie, T.; Lyon, D.; Newberger, T.; Pétron, G.; Rella, C.; Smith, M.; Wolter, S.; Yacovitch, T. I.; Tans, P. Aircraft-Based Estimate of Total Methane Emissions from the Barnett Shale Region. *Environ. Sci. Technol.* **2015**, *49* (13), 8124−8131.
(55) Ravikumar, A.; Li, Z. H.; Yang, L.; Smith, M. Developing Measurement-Informed Methane Emissions Inventory Estimates at Midstream Compressor Stations. *ChemRxiv* **2024**, 8jmtn.
(56) Weil, M.; Cooney, J.; Hossain, M.; Konieczny, M.; Leibensperger, E. M. Contributing to a Greener New York: Analysis of Methane Emissions in New York State. *J. Undergrad. Rep. Phys.* **2023**, *33* (1), No. 22471.
(57) Fredenslund, A. M.; Mønster, J.; Kjeldsen, P.; Scheutz, C. Development and Implementation of a Screening Method to Categorise the Greenhouse Gas Mitigation Potential of 91 Landfills. *Waste Manage.* **2019**, *87*, 915−923.
(58) Mønster, J. G.; Samuelsson, J.; Kjeldsen, P.; Rella, C. W.; Scheutz, C. Quantifying Methane Emission from Fugitive Sources by Combining Tracer Release and Downwind Measurements − A Sensitivity Analysis Based on Multiple Field Surveys. *Waste Manage.* **2014**, *34* (8), 1416−1428.
(59) Rella, C. W.; Tsai, T. R.; Botkin, C. G.; Crosson, E. R.; Steele, D. Measuring Emissions from Oil and Natural Gas Well Pads Using the Mobile Flux Plane Technique. *Environ. Sci. Technol.* **2015**, *49* (7), 4742−4748.
(60) Martin, D. O. Comment On 'The Change of Concentration Standard Deviations with Distance'. *J. Air Pollut Control Assoc* **1976**, *26* (2), 145−147.
(61) Riddick, S. N.; Mauzerall, D. L.; Celia, M.; Harris, N. R. P.; Allen, G.; Pitt, J.; Staunton-Sykes, J.; Forster, G. L.; Kang, M.; Lowry, D.; Nisbet, E. G.; Manning, A. J. Methane Emissions from Oil and Gas Platforms in the North Sea. *Atmos Chem. Phys.* **2019**, *19* (15), 9787−9796.
(62) Mohammadloo, T. H.; Jones, M.; van de Kerkhof, B.; Dawson, K.; Smith, B. J.; Conley, S.; Corbett, A.; IJzermans, R. Quantitative Estimate of Several Sources of Uncertainty in Drone-Based Methane Emission Measurements. *Atmos Meas Tech* **2025**, *18* (5), 1301−1324.
(63) Foulds, A.; Allen, G.; Shaw, J. T.; Bateson, P.; Barker, P. A.; Huang, L.; Pitt, J. R.; Lee, J. D.; Wilde, S. E.; Dominutti, P.; Purvis, R. M.; Lowry, D.; France, J. L.; Fisher, R. E.; Fiehn, A.; Pühl, M.; Bauguitte, S. J. B.; Conley, S. A.; Smith, M. L.; Lachlan-Cope, T.; Pisso, I.; Schwietzke, S. Quantification and Assessment of Methane Emissions from Offshore Oil and Gas Facilities on the Norwegian Continental Shelf. *Atmos Chem. Phys.* **2022**, *22* (7), 4303−4322.
(64) Moore, D. P.; Li, N. P.; Wendt, L. P.; Castañeda, S. R.; Falinski, M. M.; Zhu, J.-J.; Song, C.; Ren, Z. J.; Zondlo, M. A. Underestimation of Sector-Wide Methane Emissions from United States Wastewater Treatment. *Environ. Sci. Technol.* **2023**, *57* (10), 4082−4090.
(65) Lan, X.; Talbot, R.; Laine, P.; Torres, A. Characterizing Fugitive Methane Emissions in the Barnett Shale Area Using a Mobile Laboratory. *Environ. Sci. Technol.* **2015**, *49* (13), 8139−8146.
(66) Delkash, M.; Chow, F. K.; Imhoff, P. T. Diurnal Landfill Methane Flux Patterns across Different Seasons at a Landfill in Southeastern US. *Waste Management* **2022**, *144*, 76−86.
(67) Wang, X.; Jia, M.; Lin, X.; Xu, Y.; Ye, X.; Kao, C. M.; Chen, S. A Comparison of CH4, N2O and CO2 Emissions from Three Different Cover Types in a Municipal Solid Waste Landfill. *J. Air Waste Manage Assoc* **2017**, *67* (4), 507−515.
(68) Xu, L.; Lin, X.; Amen, J.; Welding, K.; McDermitt, D. Impact of Changes in Barometric Pressure on Landfill Methane Emission. *Global Biogeochem Cycles* **2014**, *28* (7), 679−695.
(69) Spokas, K. A.; Bogner, J.; Corcoran, M. Modeling Landfill CH4 Emissions: CALMIM International Field Validation, Using CALMIM to Simulate Management Strategies, Current and Future Climate Scenarios. *Elementa* **2021**, *9* (1), No. 00050.
(70) Spokas, K.; Bogner, J.; Corcoran, M.; Walker, S. From California Dreaming to California Data: Challenging Historic Models for Landfill CH4 Emissions. *Elementa* **2015**, *3*, No. 000051.
(71) Spokas, K. A.; Bogner, J. E. Limits and Dynamics of Methane Oxidation in Landfill Cover Soils. *Waste Management* **2011**, *31* (5), 823−832.

https://doi.org/10.1021/acsestair.5c00145
ACS EST Air XXXX, XXX, XXX−XXX

(72) Hanson, J. L.; Yesiller, N.; Manheim, D. C. *Estimation and Comparison of Methane, Nitrous Oxide, and Trace Volatile Organic Compound Emissions and Gas Collection System Efficiencies in California Landfills*. https://ww2.arb.ca.gov/sites/default/files/2020-12/CalPoly_LFG_Study_03-30-20.pdf (accessed September 3, 2025).
(73) Spokas, K.; Bogner, J.; Chanton, J. A Process-based Inventory Model for Landfill CH4 Emissions Inclusive of Seasonal Soil Microclimate and CH4 Oxidation. *J. Geophys. Res.* **2011**, *116*, G04017.
(74) NYS DEC. *Mill Seat Landfill 2022 Annual Report*. https://extapps.dec.ny.gov/data/IF/Landfills/2022_Landfill_Annual_Reports/R8/28LS0025_Mill_Seat_msw_R8_2022.2023-2-1.AR.pdf (accessed September 3, 2025).
(75) NYS DEC. *Seneca Meadows Landfill 2022 Annual Report*. https://extapps.dec.ny.gov/data/IF/Landfills/2022_Landfill_Annual_Reports/R8/50S08_Seneca_Meadows_msw_R8_2022.2023-3-2.AR.pdf (accessed September 3, 2025).
(76) NYS DEC. *Modern Landfill, Inc. 2022 Annual Report*. https://extapps.dec.ny.gov/fs/projects/SWMF/Annual_Reports_Solid_Waste_Management_Facility/Annual_Reports_by_Activity_Type/Landfill/Landfill_Annual_Reports_-_2022/R9/32S30_Modern_Landfill_MSW_R9_2022.2023-03-02.AR.pdf (accessed September 3, 2025).
(77) Abichou, T.; Chanton, J.; Powelson, D.; Fleiger, J.; Escoriaza, S.; Lei, Y.; Stern, J. Methane Flux and Oxidation at Two Types of Intermediate Landfill Covers. *Waste Management* **2006**, *26* (11), 1305−1312.

https://doi.org/10.1021/acsestair.5c00145
ACS EST Air XXXX, XXX, XXX−XXX